Time-domain finite element formulation of porous sound absorbers based on an equivalent fluid model

Yoshida, Takumi
Okuzono, Takeshi
Sakagami, Kimihiro

ACOUSTICAL LETTER

Time-domain finite element formulation of porous sound absorbers based on an equivalent fluid model

Takumi Yoshida[1,2,*], Takeshi Okuzono[2] and Kimihiro Sakagami[2]

[1]*Technical Research Institute, Hazama Ando Corporation, 515–1 Karima, Tsukuba, 305–0822 Japan*
[2]*Environmental Acoustic Laboratory, Department of Architecture, Graduate School of Engineering, Kobe University, 1–1 Rokkodai-cho, Nada-ku, Kobe, 657–8501 Japan*

(*Received 18 June 2020, Accepted for publication 20 July 2020*)

Keywords: Extended-reacting model, FEM, Room acoustics simulation, Time domain porous absorber
PACS number: 43.55.Br, 43.55.Ka, 43.55.Dt [doi:10.1250/ast.41.837]

1. Introduction

Time-domain wave-based room acoustic modeling has attracted considerable interest in recent years. Among the various room acoustic solvers, the authors have been developing an efficient room acoustic solver using time-domain finite element method (TD-FEM) [1,2], which is extremely attractive for modeling room acoustics because of its inherent capability in dealing with complex geometry. Fundamentally, the acoustic TD-FEM uses a locally reacting equivalent impedance model for treating sound absorption effects at boundaries because of its easy implementation with a low associated computational cost. However, the model uses constant real-valued surface impedance at the frequency of interest where the frequency-dependence and incidence-angle-dependence of absorption characteristics of materials are neglected. Therefore, constructing an adequate extended-reacting sound absorber model is an extremely important topic for enhancing the accuracy of room acoustic prediction. Although earlier studies [3,4] have incorporated an extended-reaction model of permeable membrane absorbers into the TD-FEM, it remains an unsolved issue for other sound absorbers such as porous absorbers. The analyses described herein are undertaken to construct a time-domain finite element (FE) model of the extended-reacting porous absorbers based on an equivalent fluid model [5,6].

In the equivalent fluid model, sound absorption in porous materials, which derives from viscothermal dissipation, is modeled with frequency-dependent parameters such as the complex effective density. Therefore, the direct formulation of time-domain equivalent fluid model engenders a convolution integral with heavy computational cost. Zhao *et al.* [7] proposed a finite-difference time-domain algorithm dealing with the equivalent fluid using Z-transformation to avoid convolution. However, the Z-transformation requires a very small time interval value to reflect frequency-dependent properties accurately. However, an efficient recursive convolution method called an auxiliary differential equations (ADE) method [8] has been applied to model a time-domain frequency-dependent boundary condition [9,10] because the ADE method can reflect frequency-dependent properties efficiently with a rougher time interval value by solving additional differential equations with higher-order numerical solvers. The ADE method can be used to construct efficient time-domain equivalent fluid modeling. Nevertheless, no study to date has incorporated the time-domain equivalent fluid model into TD-FEM.

As described herein, this study incorporates the time-domain equivalent-fluid-based porous absorber model into TD-FEM using the ADE method. A numerical impedance tube problem validates the proposed formulation. Then the following are investigated to increase the numerical efficiency of the present method: (1) applicability of modified integration rule (MIR) [11] to reduce the inherent discretization error, called the dispersion error, and (2) improving numerical stability using implicit Runge–Kutta method for solving additional differential equations associated with the ADE method.

2. Theory

2.1. Equivalent-fluid-based finite elements in the frequency domain

In the frequency domain, the following Helmholtz equation with a complex wavenumber k_e describes sound propagation in isotropic rigid-frame porous materials as

$$(\nabla^2 + k_e^2)p = 0, \tag{1}$$

where p and ∇^2 respectively stand for the sound pressure and the Laplacian operator. Assuming a time factor $\exp(-j\omega t)$ and introducing FE approximation with rigid and vibration boundary conditions into Eq. (1) yields the semi-discretized matrix equation as

$$(\epsilon \boldsymbol{K}_p - \epsilon k_e^2 \boldsymbol{M}_p)\boldsymbol{p} = j\omega\rho_0 v_n^p \boldsymbol{W}, \tag{2}$$

where $\boldsymbol{M}_p$ and $\boldsymbol{K}_p$ respectively represent the mass matrix and the stiffness matrix in porous materials, and $\boldsymbol{p}$ and $\boldsymbol{W}$ respectively denote the sound pressure vector and the distribution vector. Also, ω and j respectively stand for the angular frequency and the imaginary unit $j^2 = -1$. v_n^p expresses the outward particle velocity at boundary. The frequency-dependent parameter ϵ is defined as ρ_0/ρ_e with air density ρ_0 and the complex effective density of porous materials ρ_e $(= \frac{Z_c k_e}{\omega})$, where Z_c is the characteristic impedance

*e-mail: yoshida.takumi@ad-hzm.co.jp

of porous materials. The time-domain expression of Eq. (2) is described as

$$\boldsymbol{M}_{\mathrm{p}}[\check{\zeta} * \ddot{\boldsymbol{p}}] + c_0^2 \boldsymbol{K}_{\mathrm{p}}[\check{\epsilon} * \boldsymbol{p}] = -\rho_0 c_0^2 \dot{v}_n^{\mathrm{p}} \boldsymbol{W}. \tag{3}$$

Here, $\check{\epsilon}$ and $\check{\zeta}$ are time-domain variables for ϵ and ζ accessed by inverse Fourier transformation, where ζ is defined as $\epsilon k_{\mathrm{e}}^2/k^2$. Here, k and c_0 are, respectively, the real wavenumber and the speed of sound in air. Additionally, the symbols $\cdot$, $\cdot\cdot$, and $*$ denote first-order and second-order time derivatives and the convolution integral. The ρ_{e} and k_{e}, which are included in the frequency-dependent parameters ζ and ϵ, are accessible with theoretical models such as the Miki model [12] and Johnson–Champoux–Allard model [6], or measured values. We use the Miki model for these quantities. Moreover, we adapt the ADE method [8] to perform the two convolution integrals in Eq. (3) with a low computational cost.

2.2. Equivalent-fluid-based finite elements in the time domain

With the ADE method, the frequency-dependent parameters ζ and ϵ are approximated using the following rational functions in the frequency domain.

$$\zeta(\omega) \approx \zeta_\infty + \sum_{i=1}^{n_{\mathrm{rp}}^\zeta} \frac{A_i^\zeta}{\lambda_i^\zeta - j\omega} + \sum_{i=1}^{n_{\mathrm{cp}}^\zeta} \left(\frac{B_i^\zeta + jC_i^\zeta}{\alpha_i^\zeta + j\beta_i^\zeta - j\omega} + \frac{B_i^\zeta - jC_i^\zeta}{\alpha_i^\zeta - j\beta_i^\zeta - j\omega} \right). \tag{4}$$

$$\epsilon(\omega) \approx \epsilon_\infty + \sum_{i=1}^{n_{\mathrm{rp}}^\epsilon} \frac{A_i^\epsilon}{\lambda_i^\epsilon - j\omega} + \sum_{i=1}^{n_{\mathrm{cp}}^\epsilon} \left(\frac{B_i^\epsilon + jC_i^\epsilon}{\alpha_i^\epsilon + j\beta_i^\epsilon - j\omega} + \frac{B_i^\epsilon - jC_i^\epsilon}{\alpha_i^\epsilon - j\beta_i^\epsilon - j\omega} \right). \tag{5}$$

Here, n_{rp} and n_{cp} respectively represent numbers of real poles and pairs of complex conjugate poles. ζ_∞, ϵ_∞, λ_i, α_i, β_i, A_i, B_i, and C_i are all real parameters. Superscripts ζ and ϵ respectively denote parameters related with ζ and ϵ. In this study, the vector fitting method [13] is used to access the parameters. Using Eqs. (4) and (5), the convolution computations of $\check{\zeta} * \ddot{\boldsymbol{p}}$ and $\check{\epsilon} * \boldsymbol{p}$ can be undertaken as

$$\check{\zeta} * \ddot{\boldsymbol{p}} \approx \zeta_\infty \ddot{\boldsymbol{p}} + \sum_{i=1}^{n_{\mathrm{rp}}^\zeta} A_i^\zeta \boldsymbol{\phi}_i^\zeta + 2 \sum_{i=1}^{n_{\mathrm{cp}}^\zeta} (B_i^\zeta \boldsymbol{\psi}_i^{\zeta(1)} + C_i^\zeta \boldsymbol{\psi}_i^{\zeta(2)}), \tag{6}$$

$$\check{\epsilon} * \boldsymbol{p} \approx \epsilon_\infty \boldsymbol{p} + \sum_{i=1}^{n_{\mathrm{rp}}^\epsilon} A_i^\epsilon \boldsymbol{\phi}_i^\epsilon + 2 \sum_{i=1}^{n_{\mathrm{cp}}^\epsilon} (B_i^\epsilon \boldsymbol{\psi}_i^{\epsilon(1)} + C_i^\epsilon \boldsymbol{\psi}_i^{\epsilon(2)}). \tag{7}$$

Here, $\boldsymbol{\phi}_i$, $\boldsymbol{\psi}_i^{(1)}$, and $\boldsymbol{\psi}_i^{(2)}$ are the auxiliary functions calculated from the following first-order ordinary differential equations as

$$\begin{aligned} &\dot{\boldsymbol{\phi}}_i^\zeta + \lambda_i^\zeta \boldsymbol{\phi}_i^\zeta = \ddot{\boldsymbol{p}}, \\ &\dot{\boldsymbol{\psi}}_i^{\zeta(1)} + \alpha_i^\zeta \boldsymbol{\psi}_i^{\zeta(1)} + \beta_i^\zeta \boldsymbol{\psi}_i^{\zeta(2)} = \ddot{\boldsymbol{p}}, \\ &\dot{\boldsymbol{\psi}}_i^{\zeta(2)} + \alpha_i^\zeta \boldsymbol{\psi}_i^{\zeta(2)} - \beta_i^\zeta \boldsymbol{\psi}_i^{\zeta(1)} = \boldsymbol{0}, \end{aligned} \tag{8}$$

and

$$\begin{aligned} &\dot{\boldsymbol{\phi}}_i^\epsilon + \lambda_i^\epsilon \boldsymbol{\phi}_i^\epsilon = \boldsymbol{p}, \\ &\dot{\boldsymbol{\psi}}_i^{\epsilon(1)} + \alpha_i^\epsilon \boldsymbol{\psi}_i^{\epsilon(1)} + \beta_i^\epsilon \boldsymbol{\psi}_i^{\epsilon(2)} = \boldsymbol{p}, \\ &\dot{\boldsymbol{\psi}}_i^{\epsilon(2)} + \alpha_i^\epsilon \boldsymbol{\psi}_i^{\epsilon(2)} - \beta_i^\epsilon \boldsymbol{\psi}_i^{\epsilon(1)} = \boldsymbol{0}. \end{aligned} \tag{9}$$

The differential equations of Eqs. (8) and (9) are solved using various numerical methods. The present paper uses Runge–Kutta method (RKM). Substituting Eqs. (6) and (7) into Eq. (3) yields the time-domain matrix equation of porous absorbers based on an equivalent fluid model as

$$\zeta_\infty \boldsymbol{M}_{\mathrm{p}} \ddot{\boldsymbol{p}} + \boldsymbol{M}_{\mathrm{p}} \boldsymbol{X}^\zeta + c_0^2 \epsilon_\infty \boldsymbol{K}_{\mathrm{p}} \boldsymbol{p} + c_0^2 \boldsymbol{K}_{\mathrm{p}} \boldsymbol{X}^\epsilon = -\rho_0 c_0^2 \dot{v}_n^{\mathrm{p}} \boldsymbol{W}, \tag{10}$$

with

$$\boldsymbol{X}^\zeta = \sum_{i=1}^{n_{\mathrm{rp}}^\zeta} A_i^\zeta \boldsymbol{\phi}_i^\zeta + 2 \sum_{i=1}^{n_{\mathrm{cp}}^\zeta} (B_i^\zeta \boldsymbol{\psi}_i^{\zeta(1)} + C_i^\zeta \boldsymbol{\psi}_i^{\zeta(2)}), \tag{11}$$

$$\boldsymbol{X}^\epsilon = \sum_{i=1}^{n_{\mathrm{rp}}^\epsilon} A_i^\epsilon \boldsymbol{\phi}_i^\epsilon + 2 \sum_{i=1}^{n_{\mathrm{cp}}^\epsilon} (B_i^\epsilon \boldsymbol{\psi}_i^{\epsilon(1)} + C_i^\epsilon \boldsymbol{\psi}_i^{\epsilon(2)}). \tag{12}$$

2.3. Time marching scheme for air-porous coupled domains

Sound propagation in the air domain is described with the wave equation as shown below.

$$\frac{\partial^2 p}{\partial t^2} - c_0^2 \nabla^2 p = 0 \tag{13}$$

Applying the FE discretization and inserting the rigid and vibration boundary conditions engender the following semi-discretized matrix equation as

$$\boldsymbol{M} \ddot{\boldsymbol{p}} + c_0^2 \boldsymbol{K} \boldsymbol{p} = -\rho_0 c_0^2 \dot{v}_n^0 \boldsymbol{W}, \tag{14}$$

where $\boldsymbol{M}$ and $\boldsymbol{K}$ respectively denote the mass matrix and the stiffness matrix in air region. Therein, v_n^0 stands for the outward particle velocity at boundary. The semi-discretized matrix equation of air-porous coupled domains is derived with the continuity condition in terms of sound pressure and particle velocity at the interface of both domains as

$$\boldsymbol{M}_{\mathrm{c}} \ddot{\boldsymbol{p}} + c_0^2 \boldsymbol{K}_{\mathrm{c}} \boldsymbol{p} = \boldsymbol{f} - \boldsymbol{M}_{\mathrm{p}} \boldsymbol{X}^\zeta - c_0^2 \boldsymbol{K}_{\mathrm{p}} \boldsymbol{X}^\epsilon, \tag{15}$$

with

$$\boldsymbol{M}_{\mathrm{c}} = \boldsymbol{M} + \zeta_\infty \boldsymbol{M}_{\mathrm{p}}, \quad \boldsymbol{K}_{\mathrm{c}} = \boldsymbol{K} + \epsilon_\infty \boldsymbol{K}_{\mathrm{p}}, \tag{16}$$

where $\boldsymbol{f}$ represents the external force vector. In the temporal direction, Eq. (15) is discretized with the fourth-order accurate Newmark β method called Fox–Goodwin method [1]. The resulting time marching scheme is expressed as

$$\left(\boldsymbol{M}_{\mathrm{c}} + \frac{c_0^2 \Delta t^2}{12} \boldsymbol{K}_{\mathrm{c}} \right) \ddot{\boldsymbol{p}}^{n+1} = \boldsymbol{f}^{n+1} - c_0^2 \boldsymbol{K}_{\mathrm{c}} \boldsymbol{Q} - \boldsymbol{M}_{\mathrm{p}} \boldsymbol{X}^{\zeta,n+1} - c_0^2 \boldsymbol{K}_{\mathrm{p}} \boldsymbol{X}^{\epsilon,n+1}, \tag{17}$$

$$\boldsymbol{p}^{n+1} = \boldsymbol{p}^n + \Delta t \dot{\boldsymbol{p}}^n + \Delta t^2 \left(\frac{5}{12} \ddot{\boldsymbol{p}}^n + \frac{1}{12} \ddot{\boldsymbol{p}}^{n+1} \right), \tag{18}$$

$$\dot{\boldsymbol{p}}^{n+1} = \dot{\boldsymbol{p}}^n + \frac{\Delta t}{2} (\ddot{\boldsymbol{p}}^n + \ddot{\boldsymbol{p}}^{n+1}), \tag{19}$$

with

$$\boldsymbol{Q} = \boldsymbol{p}^n + \Delta t \dot{\boldsymbol{p}}^n + \frac{5\Delta t^2}{12}\ddot{\boldsymbol{p}}^n. \tag{20}$$

Hereinafter, the implicit equation of Eq. (17) is solved using a preconditioned iterative solver called conjugate gradient method with diagonal scaling. The convergence tolerance is set as 10^{-4}.

3. Numerical experiments

We examined the validity of proposed method via the three-dimensional impedance tube problems, by which surface impedance z of porous sound absorbers were computed based on the transfer function method. The validation includes investigations from an important aspect in terms of numerical efficiency of the present scheme. We tested the applicability of MIR to reduce the dispersion error in porous domain, and implicit RKM to improve the accuracy and stability of the scheme. We assumed porous absorbers of two kinds (PA-1 and PA-2): PA-1 is a rigid-backed porous material with thickness of 0.025 m and flow resistivity of 13,000 Pa s/m^2; PA-2 consists of the same porous material as PA-1 but it has an air cavity of 0.05 m depth behind the porous material. Figure 1 presents FE meshes of the impedance tube including the sound absorbers of PA-1 and PA-2. For porous materials in PA-1 and PA-2, the frequency-dependent parameters ζ and ϵ were approximated, respectively, by the rational functions with only real poles of $n_{\mathrm{rp}}^{\zeta} = 6$ and $n_{\mathrm{rp}}^{\epsilon} = 4$. Figure 2 presents comparisons of ζ and ϵ between the theoretical values and the fitted rational function model, where the rational function model shows excellent agreement with the theory. As an initial condition, we considered plane wave incidence at the tube inlet with the Gaussian pulse waveform having an upper-limit frequency of 10 kHz. Both models were discretized spatially by eight-node cubic elements of 0.005 m, having spatial resolution of 6.87 points per wavelength at 10 kHz. The sound speed c_0 was set as 343.7 m/s.

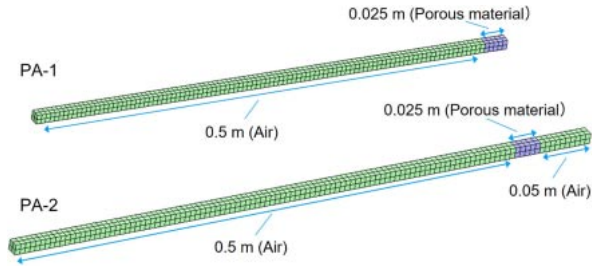

Fig. 1 Finite element model of impedance tube including porous absorbers PA-1 and PA-2.

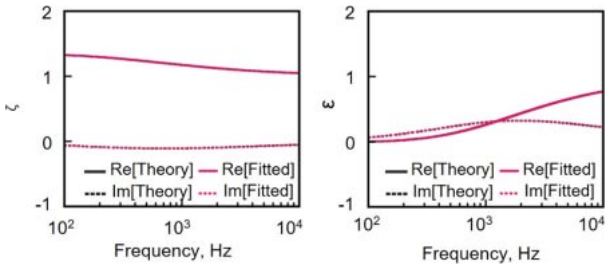

Fig. 2 Comparisons of frequency-dependent parameters ζ (Left) and ϵ (Right) calculated using the theory and the fitted rational function model.

3.1. Applicability of modified integration rules to the porous domain

For acoustic FEM in the frequency domain, MIR was applied to reduce the dispersion error. The MIR is the Gauss–Legendre numerical quadrature with modified integration points. The earlier study [11] presents that the use of modified integration points of $\alpha_{\mathrm{M}} = \pm\sqrt{2/3}$ in element mass and stiffness matrices calculations instead of conventional points of $\alpha_{\mathrm{C}} = \pm\sqrt{1/3}$ results in much better accuracy in terms of spatial discretization in air-porous coupled problems. However, the applicability of MIR in time-domain analysis is examined only for air domains. Therefore, its applicability to the porous region remains unclear. Here, we tested the applicability by comparing results calculated using α_{M} and α_{C}. In the analysis, we set Δt as $\Delta t = l\Delta t_{\mathrm{c}}$, where Δt_{c} is the critical time interval for air region, which is defined as $\Delta t_{\mathrm{c}} = \frac{h}{c_0\sqrt{3}}$ [1] with an element size h in cubic elements. Therein, l is a numerically accessed parameter necessary for stable computation. The four-stage fourth-order explicit RKM [14] is used for solving differential equations of Eqs. (8) and (9).

Figure 3 presents comparisons of z in cases with PA-1 and PA-2 calculated using the theory [5] and the proposed TD-FEM with modified integration point α_{M} and conventional integration point α_{C}. The proposed method with α_{M} shows better agreement with theory for the two cases. The proposed method with α_{C} shows marked discrepancy at higher frequencies, where frequencies at which peaks and dips occur are shifted to higher frequencies than those which are expected from theory. The results showed that the proposed method with MIR is valid to analyze sound propagations in the air-porous coupled domain, and to analyze them more efficiently than when using the method with conventional integration points. However, we observed worse stability for

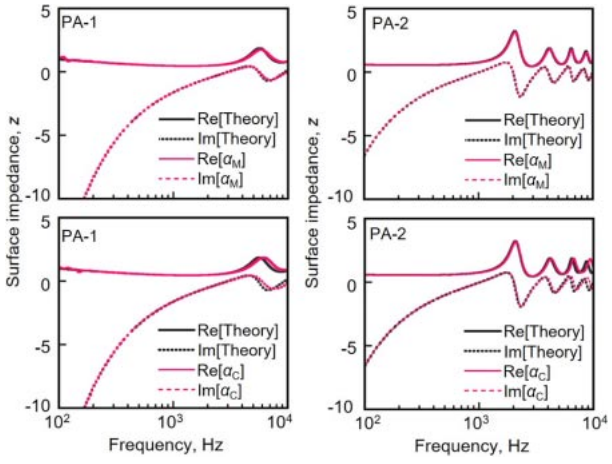

Fig. 3 Comparisons of surface impedance z calculated using the theory and the proposed TD-FEM with a modified integration point α_{M} (Upper) and conventional integration point α_{C} (Lower) in cases of PA-1 (Left) and PA-2 (Right).

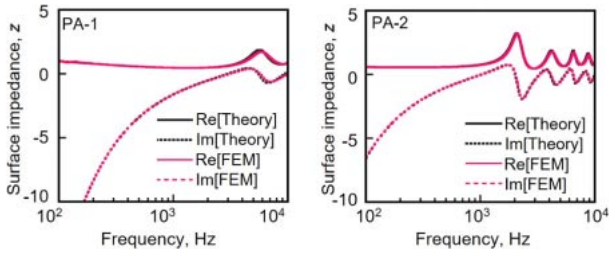

Fig. 4 Comparisons of surface impedance z of PA-1 (Left) and PA-2 (Right) calculated using theory and the proposed TD-FEM with implicit RKM.

the proposed scheme. For these experiments, $l = 0.5$ was found to be necessary for stable computations.

3.2. Improving stability with implicit RKM

In general, implicit RKM has better stability than explicit RKM but involves larger computational cost for the solution of linear equation. However, the resulting linear equation for the auxiliary functions has only vectors, which can be easily transformed to an explicit form using simple four arithmetic operations in advance. Here, we attempted to improve the stability of the proposed method using two-stage fourth-order implicit RKM [15] with comparable computational complexity to the explicit RKM to solve Eqs. (8) and (9). We performed the same numerical experiments as in **3.1.** with modified integration points α_{M}. Figure 4 presents comparisons of z of PA-1 and PA-2 calculated using the theory and the proposed method with implicit RKM. Good agreement between the theoretical results and the numerical results can be found. More importantly the results were obtained with improved stability of $l = 0.9$ without losing accuracy. The implicit RKM can achieve same accuracy as the explicit RKM with 1.8 times larger Δt and with 1.46–1.74 times faster computational time than the explicit RKM.

4. Conclusion

This paper presents a proposal of an implicit time domain finite element formulation of extended-reacting porous sound absorbers based on an equivalent-fluid-based model. The ADE method was applied to address frequency-dependent parameters ζ and ϵ related to porous materials efficiently. The numerical experiments validated the presented formulation, which revealed also that the proposed formulation with MIR can analyze sound propagation in air-porous coupled problems in a broad frequency range with a single computation. Moreover, results clarified that the use of implicit RKM for solving additional differential equations accompanied with the ADE method drastically improved numerical stability compared with the case of using explicit RKM while maintaining sufficient accuracy.

References

[1] T. Okuzono, T. Otsuru, R. Tomiku and N. Okamoto, "Application of modified integration rule to time-domain finite-element acoustic simulation of rooms," *J. Acoust. Soc. Am.*, **132**, 804–813 (2012).
[2] T. Yoshida, T. Okuzono and K. Sakagami, "Time domain room acoustic solver with fourth-order explicit FEM using modified time integration," *Appl. Sci.*, **10**, 3750 (2020).
[3] T. Yoshida, T. Okuzono and K. Sakagami, "A three-dimensional time-domain finite element method based on first-order ordinary differential equations for treating permeable membrane absorbers," *Proc. 25th Int. Congr. on Sound Vib.*, 838, 7 pages (2018).
[4] T. Okuzono, N. Shimizu and K. Sakagami, "Predicting absorption characteristics of single-leaf permeable membrane absorbers using finite element method in a time domain," *Appl. Acoust.*, **151**, 172–182 (2019).
[5] J. F. Allard and N. Atalla, "Acoustic impedance at normal incidence of fluids. Substitution of a fluid layer for a porous layer," in *Propagation of Sound in Porous Media: Modeling Sound Absorbing Materials*, 2nd ed. (John Wiley & Sons, Chichester, 2009), Chap. 2, pp. 15–27.
[6] J. F. Allard and N. Atalla, "Sound propagation in porous materials having a rigid frame," in *Propagation of Sound in Porous Media: Modeling Sound Absorbing Materials*, 2nd ed. (John Wiley & Sons, Chichester, 2009), Chap. 5, pp. 73–109.
[7] J. Zhao, M. Bao, X. Wang, H. Lee and S. Sakamoto, "An equivalent fluid model based finite-difference time-domain algorithm for sound propagation in porous material with rigid frame," *J. Acoust. Soc. Am.*, **143**, 130–138 (2018).
[8] D. Dragna, P. Pineau and P. Blanc-Benon, "A generalized recursive convolution method for time-domain propagation in porous media," *J. Acoust. Soc. Am.*, **138**, 1030–1042 (2015).
[9] F. Pind, A. P. Engsig-Karup, C. H. Jeong, J. S. Hesthaven, M. S. Mejling and J. Strømann-Anderson, "Time domain room acoustic simulations using the spectral element method," *J. Acoust. Soc. Am.*, **145**, 3299–3310 (2019).
[10] H. Wang and M. Hornikx, "Time-domain impedance boundary condition modeling with the discontinuous Galerkin method for room acoustics simulations," *J. Acoust. Soc. Am.*, **147**, 2534–2546 (2020).
[11] T. Okuzono and K. Sakagami, "Dispersion error reduction of absorption finite elements based on equivalent fluid model," *Acoust. Sci. & Tech.*, **39**, 362–365 (2018).
[12] Y. Miki, "Acoustical properties of porous materials — Modification of Delany-Bazley models —," *J. Acoust. Soc. Jpn. (E)*, **11**, 19–24 (1990).
[13] B. Gustavsen and A. Semlyen, "Rational approximation of frequency domain responses by vector fitting," *IEEE Trans. Power Deliv.*, **14**, 1052–1061 (1999).
[14] P. O. J. Scherer, "Equations of motion," in *Computational Physics: Simulation of Classical and Quantum Systems*, 3rd ed. (Springer Nature, Berlin/Heidelberg, 2017), Chap. 13, pp. 292–303.
[15] J. C. Butcher, "Implicit Runge–Kutta processes," *Math. Comput.*, **18**, 50–64 (1964).